Zeitschrift für anorganische und allgemeine Chemie

Journal of Inorganic and General Chemistry
ZAAC
Zeitschrift für anorganische und allgemeine Chemie

RESEARCH ARTICLE OPEN ACCESS

Characterization of the Carbonyl Metalates $[Mn_2(CO)_8]^{2-}$ and $[W_2(CO)_8]^{4-}$ Featuring *M*=*M* Double Bonds

Michael Witzmann | Franz Wieberneit | Nikolaus Korber

Institute of Inorganic Chemistry, University of Regensburg, Regensburg, Germany

Correspondence: Nikolaus Korber (nikolaus.korber@ur.de)

Received: 18 August 2025 | **Revised:** 28 November 2025 | **Accepted:** 3 December 2025

Keywords: carbonyl complex | liquid ammonia | QTAIM | transition metalate | X-ray diffraction

ABSTRACT

The crystal structures of $[Rb[2.2.2]crypt]_2[Mn_2(CO)_8] \cdot 4NH_3$ and $[K[18]crown\text{-}6]_2K_2[W_2(CO)_8] \cdot 14NH_3$ are reported, containing the first homoleptic dinuclear carbonyl metalates featuring metal–metal double bonds. $[Mn_2(CO)_8]^{2-}$ and $[W_2(CO)_8]^{4-}$ are isostructural and isoelectronic to the elusive $[Fe_2(CO)_8]$. Quantum chemical calculations and QTAIM analysis confirm the metallic bonding character, as well as differences in terminal and bridging carbonyl ligands.

1 | Introduction

Ever since the synthesis of $[Ni(CO)_4]$ by *L. Mond* in 1890, transition metal carbonyl complexes have been intensively studied [1]. Their remarkable catalytic properties for organic transformation reactions make them indispensable catalysts in the chemical industry as well as in university laboratories [2, 3]. However, transition metal carbonyl complexes are of interest not only for their potential application but also for their structural diversity. Homoleptic carbonyl complexes can be cationic, neutral or anionic [4–6]. Negatively charged carbonyl metalates with a single transition metal atom have been synthesized for group 4–10 metals with formal oxidation states for the metal centers from –I to –IV [7]. Additionally, the formation of metal–metal bonds results in the linkage to dimers or larger, multinuclear clusters, containing bridging carbonyl ligands [8, 9]. Multinuclear metalates are mostly observed for the heavier group 8–10 metals. With respect to dinuclear anions, $[M_2(CO)_{10}]^{2-}$ (*M* = Cr, Mo, W) [10, 11], $[M_2(CO)_9]^{2-}$ (*M* = Mn, Tc, Re) [7, 12], $[Fe_2(CO)_8]^{2-}$ [13], and $[Ni_2(CO)_6]^{2-}$ [14] are known, which feature metal centers in the formal oxidation state –I. Out of those, only the anions from group 6 and the nickel anion have been structurally characterized by X-ray diffraction. All of these dimers contain a metal–metal single bond, which is in accordance with the 18-valence electron rule and supported by the *M*–*M* distances. Furthermore, one can think of isoelectronic varieties of these complexes by adding an additional metal–metal bond and removing either a carbonyl ligand or two negative charges. Such species have only been observed spectroscopically in low temperature matrices. For example, *Poliakoff* and *Turner* were able to briefly generate $[Fe_2(CO)_8]$ via UV irradiation at 20 K [15]. *R. Hoffmann* already proposed in his Nobel lecture that this compound can be related to the simple ethylene molecule using the isolobal principle [16]. The $Fe(CO)_4$ fragment is isolobal to the CH_2 fragment, which leads to the formation of $[(CO)_4Fe{=}Fe(CO)_4]$ and $H_2C{=}CH_2$, respectively. Further observations led to the identification of a structure with two bridging carbonyl ligands, which was later supported using quantum chemical calculations [17, 18]. When moving from iron to group 7 or group 6 metals, anionic complexes in the form of $[M_2(CO)_8]^{n-}$ (*M* = Mn, Tc, Re; n = 2; *M* = Cr, Mo, W; n = 4) containing *M*=*M* double bonds can be expected. In this article we present two ammoniate crystal structures containing the first two representatives of this type, $[Mn_2(CO)_8]^{2-}$ and $[W_2(CO)_8]^{4-}$.

In Memoriam of Prof. Dr. Harald Hillebrecht.

2 | Results and Discussion

2.1 | Crystal Structures of [Rb [2.2.2] crypt]$_2$[$Mn_2(CO)_8$] · 4NH_3 and [K [18]crown-6]$_2$$K_2$[$W_2(CO)_8$] · 14$NH_3$

Black plates of [Rb [2.2.2]crypt]$_2$[$Mn_2(CO)_8$] · 4NH_3 (1) could obtained from the reduction $Mn_2(CO)_{10}$ by elemental rubidium in liquid ammonia in the presence of [2.2.2]crypt. [K [18]crown-6]$_2$$K_2$[$W_2(CO)_8$] · 14$NH_3$ (2) was obtained as orange needles from a solution of $W(CO)_4$(tmeda), K_4Pb_9, [18]crown-6 and [2.2.2] crypt. The $[Pb_9]^{4-}$ anion in K_4Pb_9 is known to be potent reducing agent in liquid ammonia [19]. Both solutions contained leftover reactants or other noncrystalline products. The procedures are therefore not suitable for a selective synthesis.

The crystal structures of (1) and (2) contain the homoleptic dinuclear carbonyl metalates $[Mn_2(CO)_8]^{2-}$ and $[W_2(CO)_8]^{4-}$, respectively. (see Figure 1).

Each metal atom is coordinated by three terminal and one bridging carbonyl ligand in the asymmetric unit. The inversion center in the center of each dinuclear anion generates the other half of the anion. This leads to a staggered orientation of the CO ligands. The *M*−C distances to the terminal carbonyl ligands range from 1.782(2) Å to 1.795(2) Å for $[Mn_2(CO)_8]^{2-}$ and from 1.9188(18) Å to 1.9716(18) Å for $[W_2(CO)_8]^{4-}$. The *M*−C distances of bridging carbonyl ligands are elongated and range from 1.947(2) Å to 2.0457(19) Å for $[Mn_2(CO)_8]^{2-}$ and 2.1534(17) Å to 2.2002(17) Å for $[W_2(CO)_8]^{4-}$. This is in accordance with interatomic distances of mononuclear manganate [20] and tungstate [11] carbonyl complexes, as well as data for other metal bridging carbonyl groups [21].

The *M*−*M* distances of both anions are of particular interest. They are significantly shorter than the metal−metal single bond distances in the homoleptic carbonyl complex analogs $Mn_2(CO)_{10}$ and $[W_2(CO)_{10}]^{2-}$, respectively. (see Table 1) There is no structural data of a carbonyl manganate dimer for comparison.

This observation is indicative of metal−metal double bonds between the transition metal atoms. Furthermore, the distances are in the range of other comparable double bond interactions in manganese and tungsten compounds [23, 24]. These shared bonding electrons allow for the fulfillment of the 18-electron rule for both transition metal atoms. The topic of attributing *M*−*M* bonds and the corresponding bond order in dinuclear complexes in the presence of bridging carbonyl ligands has been the subject of some debate. Based on calculations that show the absence of *M*−*M* bonding interactions in symmetrically carbonyl bridged dinuclear complexes, it has been suggested that the bridging interaction can be viewed not only as a 3c−2e interaction but also as two 2c−2e bonds [25]. This is possible because the bridging carbonyl ligands can act as both σ−donors and π−acceptors towards the two metal centers. The difference in electron counting methods would replace one *M*−*M* bond per two bridging carbonyl ligands while still fulfilling the 18-electron rule. Therefore, it has to be noted that the interactions in $[Mn_2(CO)_8]^{2-}$ and $[W_2(CO)_8]^{4-}$ can also be described as *M*−*M* single bonds. However, since the distances between the metal centers are in accordance with the aforementioned double bonding interactions, which use the conventional electron counting method, we attribute a *M*=*M* double bond.

This makes $[Mn_2(CO)_8]^{2-}$ and $[W_2(CO)_8]^{4-}$ isoelectronic as well as isostructural to the elusive $[Fe_2(CO)_8]$ and the first structurally characterized homoleptic carbonyl metalate dinuclear species containing a *M*=*M* double bond. Formally, the oxidation states of the metal centers are −I for Mn and −II for W, whereas the previously observed dinuclear species exclusively feature metal centers in the formal oxidation state −I [7].

The negative charge of the anions is compensated by alkali metal cations. The rubidium cation position in (1) is chelated in a [2.2.2]crypt molecule with no further coordination partners. The remaining space in the crystal structure is occupied by four ammonia molecules. The crystal structure of (2) contains two separate potassium cation positions. K1 is directly coordinated by four carbonyl ligands of two different anions. The remaining coordination sphere is filled by two ammonia molecules and one oxygen atom from an [18]crown-6 molecule. K2 is chelated in the crown ether and additionally coordinated by three ammonia molecules and one carbonyl ligand. (for a detailed depiction see SI, Figure S2).

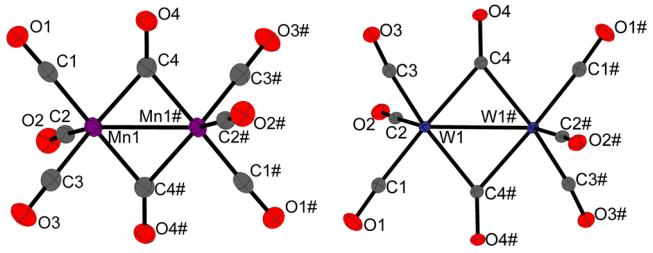

FIGURE 1 | Anionic units $[Mn_2(CO)_8]^{2-}$ (left) and $[W_2(CO)_8]^{4-}$ (right) in (1) and (2), respectively. Displacement ellipsoids are shown at 50% probability. Symmetry codes #:−X, 1−Y, 1−Z (left); #:1−X,−Y, 1−Z (right).

2.2 | Quantum Chemical Calculations

Further insight into the character of the chemical bonding in $[Mn_2(CO)_8]^{2-}$ and $[W_2(CO)_8]^{4-}$ can be gained from quantum chemical investigations and (QTAIM) quantum theory of atoms in molecules analysis. The optimized geometries and the resulting calculated interatomic distances are remarkably similar to those observed in the crystal structure. (for detailed information see SI, Figure S4 and Table S3) Based on these results, the Laplacian of the electron density $\Delta^2\rho$ can be calculated, which is depicted in Figure 2 within the *M*−*M*−C plane and along the *M*−*M* bond paths for both anions. $\Delta^2\rho$ in between the metal atoms is always positive but approaches

TABLE 1 | Comparison of the *M*−*M* distances of the anions in (1) and (2) with $Mn_2(CO)_{10}$ and $[W_2(CO)_{10}]^{2-}$.

	$[Mn_2(CO)_8]^{2-}$	Mn_2CO_{10} [22]	$[W_2(CO)_8]^{4-}$	$[W_2(CO)_{10}]^{2-}$ [11]
d(*M*−*M*)/Å	2.5053(5)	2.923	2.79782(13)	3.1106(6)

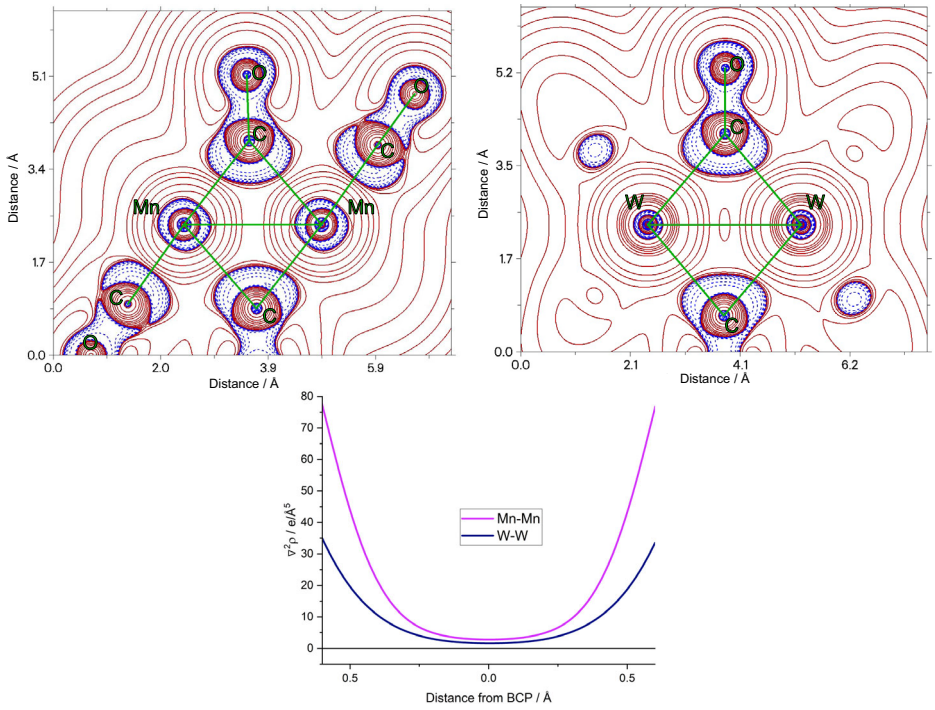

FIGURE 2 | Laplacian of the electron density within the Mn–Mn–C plane in $[Mn_2(CO)_8]^{2-}$ (top left) and within the W–W–C plane in $[W_2(CO)_8]^{4-}$ (top right) with negative values shown in blue and positive values shown in red. Laplacian of the electron density along the respective *M*–*M* bond paths (bottom).

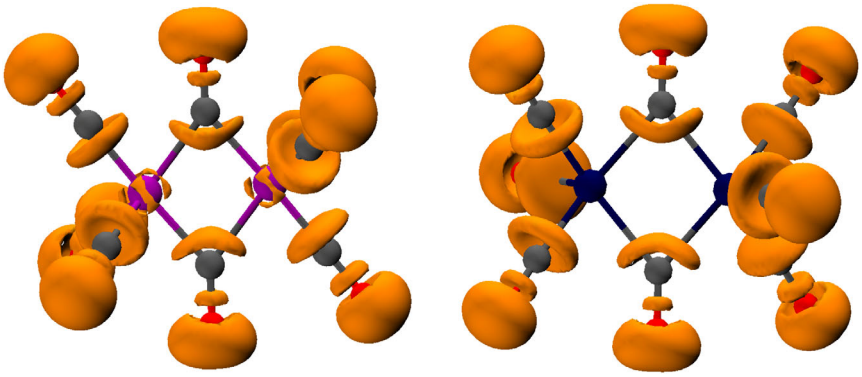

FIGURE 3 | Isosurfaces of the ELF of $[Mn_2(CO)_8]^{2-}$ (left) and $[W_2(CO)_8]^{4-}$ (right) at $\eta = 0.8$.

a value of 0. This is expected for metal–metal bonding interactions [26]. In contrast to covalent bonding, the electron density along the bond path is low and delocalized. The lone pairs of the CO ligands are visible as negative regions of $\Delta^2\rho$ oriented towards the central metal atoms. In the case of the bridging carbonyl ligands this region is larger to allow for the donation of electron density towards both metal atoms. The same trend can be observed in the ELF of $[Mn_2(CO)_8]^{2-}$ and $[W_2(CO)_8]^{4-}$, which is shown in Figure 3. Isosurfaces at η = 0.8 reveal the distorted trisynaptic basins in the *M*–*M*–C plane. In contrast, terminal carbonyl ligands show disynaptic basins along the C–*M* bonds. This visualizes the more delocalized electron density of the bridging carbonyl ligands. Additionally, the disynaptic basins of the C–O bonds and monosynaptic basins of the oxygen lone pairs are present for all CO groups, as expected for carbonyl metalate anions [27].

3 | Conclusion

The compounds [Rb [2.2.2]crypt]$_2$[$Mn_2(CO)_8$] · 4NH_3 and [K [18] crown-6]$_2$$K_2$[$W_2(CO)_8$] · 14$NH_3$ contains the first structurally characterized homoleptic carbonyl metalate dinuclear species containing a *M*=*M* double bond. $[Mn_2(CO)_8]^{2-}$ and $[W_2(CO)_8]^{4-}$ are both isoelectronic and isostructural to the elusive $[Fe_2(CO)_8]$. The results of quantum chemical investigations verify the expected metal–metal bonding interactions. It can also be confirmed that the lone pairs of bridging carbonyl ligands are delocalized in the *M*–*M*–C plane.

4 | Experimental Section

All operations were carried out in an argon gas atmosphere using standard Schlenk techniques. Liquid ammonia was dried and

stored over sodium for at least 48 h. [18]crown-6 was purified by sublimation before use. Elemental potassium was purified by liquid segregation. Elemental Rubidium was synthesized from RbCl and Ca, following the general procedure of *Hackspill* [28] and purified by distillation. $Mn_2(CO)_{10}$ (*abcr*, 98%), [2.2.2]crypt (*Sigma–Aldrich*, 98%) and elemental lead (*Sigma–Aldrich*, 99%) were used as supplied. Due to the difficulties of working in liquid ammonia and only small amounts of crystalline products, no further characterization techniques besides single crystal X-ray diffraction (SCXRD) studies were possible.

4.1 | Synthesis of K_4Pb_9

Potassium (154.8 mg, 3.9 mmol) and lead (1845.8 mg, 9.0 mmol) were weighed into a tantalum ampoule, which was welded shut under an argon atmosphere. After flame sealing in a quartz-glass ampoule under vacuum, the reaction vessel was heated to 923 K with 50 K/h and held at that temperature for 24 h before cooling to room temperature with 20 K/h.

4.2 | Synthesis of $W(CO)_4$(tmeda)

The procedure is based on a method by *King* and *Fronzaglia* [29]. $W(CO)_6$ (5.0 g, 14.2 mmol), tetramethylethylenediamine (5 mL, 39.0 mmol), 80 mL *n*-decane and a few mL of *n*-hexane were refluxed for 27 h. After crystallization at 253 K over night, the resulting crystals were washed three times with *n*-hexane and dichloromethane. ^{13}C NMR (400 MHz, $CDCl_3$): δ = 61.94 ppm (s, 2 C), δ = 57.73 ppm (s, 4 C).

4.3 | Synthesis of [Rb [2.2.2]crypt]$_2$[$Mn_2(CO)_8$] · 4NH_3 (1)

$Mn_2(CO)_{10}$ (50 mg, 0.128 mmol), Rb (65.75 mg, 0.769 mmol) and [2.2.2]crypt (96.54 mg, 0.256 mmol) were dissolved in anhydrous liquid ammonia. The resulting dark blue solution turned to a yellowish red after 3 days. After further storage at 233 K for 20 months, black plates of (1) could be isolated and characterized by SCXRD.

4.4 | Synthesis of [K [18]crown-6]$_2K_2$[$W_2(CO)_8$] · 14NH_3 (2)

A solid state material with the nominal composition K_4Pb_9 (50 mg, 0.025 mmol), $W(CO)_4$(tmeda) (10.2 mg, 0.025 mmol) [18]crown-6 (16.3 mg, 0.062 mmol) and [2.2.2]crypt (14.0 mg, 0.037 mmol) were dissolved in anhydrous liquid ammonia. After storage of the resulting dark green solution at 233 K for 2 months, orange needles of (2) could be isolated and characterized by SCXRD.

4.5 | SCXRD studies

Both (1) and (2) are sensitive to moisture, air, and temperature. After cooling in an ethanol/dry ice bath, a small amount of crystals was transferred directly from the mother liquid into liquid nitrogen stream-cooled perfluoroether oil. A suitable single crystal was isolated and subsequently transferred onto the goniometer using a MiTeGen loop cooled in liquid nitrogen during the transport. The crystal structure was recorded on an Rigaku Synergy-DW with a sealed-tube Cu/Mo-X-ray source and a 135 mm Atlas S2 CCD detector. Data collection was carried out at 123 K. For data reduction, *CrysAlisPro* [30] was used. The structure was solved using *ShelXT* [31] and refined with *ShelXL* [32]. For visualization purposes *Olex^2 1.5* [33] was used and figures were drawn up with *Diamond 5* [34] using displacement ellipsoids at the 50% probability level.

4.6 | Crystal Data for [Rb [2.2.2]crypt]$_2$[$Mn_2(CO)_8$] · 4NH_3

M = 1326.01 g·mol^{-1}, space group = $P2_1/c$, a = 11.66020(10) Å, b = 17.3483(2) Å, c = 14.5706(2) Å, β = 90.5060(10)°, V = 2947.29(6) Å^3, Z = 2, ρ_{calc} = 1.494 g·cm^{-3}, μ = 6.126 mm^{-1}, F(000) = 1376.0, 40 743 collected reflections, 5349 independent reflections, R_{int} = 3.79%, R_1 = 2.50%, ωR_2 = 6.85% for all data, GooF = 1.048, $\Delta\rho_{max}$ = 0.67 e·Å^{-3}, $\Delta\rho_{min}$ = −0.39 e·Å^{-3}.

4.7 | Crystal Data for [K [18]crown-6]$_2K_2$[$W_2(CO)_8$] · 14NH_3

M = 1497.13 g·mol^{-1}, space group = $P\bar{1}$, a = 8.61320(10) Å, b = 12.57300(10) Å, c = 15.03010(10) Å, α = 70.3380(10) Å, β = 88.4210(10)°, γ = 87.1220(10) Å, V = 1530.73(3) Å^3, Z = 1, ρ_{calc} = 1.624 g·cm^{-3}, μ = 4.099 mm^{-1}, F(000) = 746.0, 27 427 collected reflections, 11 593 independent reflections, R_{int} = 2.29%, R_1 = 2.09%, ωR_2 = 5.29% for all data, GooF = 1.056, $\Delta\rho_{max}$ = 1.24 e·Å^{-3}, $\Delta\rho_{min}$ = −0.61 e·Å^{-3}.

Crystallographic data for the compounds has been deposited in the Cambridge Crystallographic Data Centre, CCDC. The data can be obtained free of charge on quoting the deposition numbers CCDC-2 466 995 for (1) or CCDC-2 466 996 for (2) via https://www.ccdc.cam.ac.uk/data_request/cif, or by emailing data_request@ccdc.cam.ac.uk, or by contacting The Cambridge Crystallographic Data Centre, 12 Union Road, Cambridge CB2 1EZ, UK; fax: +44 1 223 336033.

4.8 | Computational Details

Geometry optimization and single point energy calculations were carried out using Orca 4.0 [35, 36] employing a B3LYP [37–40]/ma-ZORA-def2-TZVPP [41, 42] level of theory as well as implementing a CPCM model [43] with ammonia as the solvent. Multiwfn [44] was used for QTAIM calculations and the ELFs were visualized using VMD [45].

Acknowledgments

The authors acknowledge the funding from the DFG on the RTG 2620/1 - 426795949.

Open Access funding enabled and organized by Projekt DEAL.

Conflicts of Interest

The authors declare no conflicts of interest.

Data Availability Statement

The data that support the findings of this study are available from the corresponding author upon reasonable request.

References

1. L. Mond, C. Langer, and F. Quincke, "L.—Action of Carbon Monoxide on Nickel," *Journal of the Chemical Society Transactions* 57 (1890): 749–753.

2. W. A. Herrmann, "100 Years of Metal Carbonyls: A Serendipitous Chemical Discovery of Major Scientific and Industrial Impact," *Journal of Organometallic Chemistry* 383 (1990): 21–44.

3. V. Tomar, P. Kumar, M. Nemiwal, and R. K. Joshi, "Review on Catalytic Significance of 3d-Transition Metal-Carbonyl Complexes for General and Selective Organic Reactions," *Inorganic Chemistry Communications* 158 (2023): 111488.

4. M. Sellin and I. Krossing, "Homoleptic Transition Metal Carbonyl Cations: Synthetic Approaches, Characterization and Follow-Up Chemistry," *Accounts of Chemical Research* 56 (2023): 2776–2787.

5. G. Frenking, I. Fernández, N. Holzmann, S. Pan, I. Krossing, and M. Zhou, "Metal–CO Bonding in Mononuclear Transition Metal Carbonyl Complexes," *JACS Au* 1 (2021): 623–645.

6. M. Y. Darensbourg, in *Progress in Inorganic Chemistry* (John Wiley & Sons, Ltd, 1985): 221–274.

7. N. Wiberg, A. Hollemann, E. Wiberg, and G. Fischer, *Lehrbuch der Anorganischen Chemie* (De Gruyter, 2007).

8. C. Cesari, J.-H. Shon, S. Zacchini, and L. A. Berben, "Metal Carbonyl Clusters of Groups 8-10: Synthesis and Catalysis," *Chemical Society Reviews* 50 (2021): 9503–9539.

9. A. K. Hughes and K. Wade, "Metal–metal and Metal–ligand Bond Strengths in Metal Carbonyl Clusters," *Coordination Chemistry Reviews* 197 (2000): 191–229.

10. L. B. Handy, J. K. Ruff, and L. F. Dahl, "Structural Characterization of the Dinuclear Metal Carbonyl Anions $[M_2(CO)_{10}]^{2-}$ (M = Chromium, Molybdenum) and $[Cr_2(CO)_{10}H]^-$. Marked Stereochemical Effect of a Linearly Protonated Metal-Metal Bond," *Journal of the American Chemical Society* 92 (1970): 7312–7326.

11. G. B. Deacon, Z. Guo, P. C. Junk, and J. Wang, "Reductive Trapping of $[(OC)_5W–W(CO)_5]^{2-}$ in a Mixed-Valent SmII/III Calix[4]pyrrolide Sandwich," *Angewandte Chemie International Edition* 56 (2017): 8486–8489.

12. W. Hieber, W. Beck, and G. Zeitler, "Neuere Anschauungen über Reaktionsweisen der Metallcarbonyle, Insbesondere Des Mangancarbonyls," *Angewandte Chemie* 73 (1961): 364–368.

13. H. B. Chin, M. B. Smith, R. D. Wilson, and R. Bau, "Variations in Molecular Geometry along the Isoelectronic Series Octacarbonyldicobalt, Octacarbonyl Cobalt Ferrate 1-, and Octacarbonyl Diferrate (2-)," *Journal of the American Chemical Society* 96 (1974): 5285–5287.

14. W. Hieber, W. Kroder, and E. Zahn, "Notizen: Über Neue Mehrkernige Carbonylniccolate," *Zeitschrift Fur Naturforschung B* 15 (1960): 325–326.

15. M. Poliakoff and J. J. Turner, "Infrared Spectrum and Photochemistry of Di-Iron Enneacarbonyl in Matrices at 20 K: Evidence for the Formation of $Fe_2(CO)_8$," *Journal of the Chemical Society A: Inorganic, Physical, Theoretical* (1971): 2403–2410.

16. R. Hoffmann, "Building Bridges Between Inorganic and Organic Chemistry (Nobel Lecture)," *Angewandte Chemie International Edition* 21 (1982): 711–724.

17. S. C. Fletcher, M. Poliakoff, and J. J. Turner, "Structure and Reactions of Octacarbonyldiiron: An IR Spectroscopic Study Using Carbon-13 Monoxide, Photolysis with Plane-Polarized Light, and Matrix Isolation," *Inorganic Chemistry* 25 (1986): 3597–3604.

18. Y. Xie, H. F. Schäfer, and B. R. King, "Binuclear Homoleptic Iron Carbonyls: Incorporation of Formal Iron-Iron Single, Double, Triple, and Quadruple Bonds, $Fe_2(CO)_x$ (x = 9, 8, 7, 6)," *Journal of the American Chemical Society* 9, 8 (2000): 7-8746–8761.

19. S. Gärtner, M. Witzmann, C. Lorenz-Fuchs, R. M. Gschwind, and N. Korber, "Liquid Ammonia: More than an Innocent Solvent for Zintl Anions," *Inorganic Chemistry* 63 (2024): 20240–20249.

20. R. Seidel, B. Schnautz, and G. Henkel, "$[Mn(CO)_5]^-$, the First Square-Pyramidal Pentacarbonyl Complex in the Complex Salt $[Ph_4P][Mn(CO)_5]$, and $[Mn_3Se_2(CO)_9]^{2-}$, the First Mixed Carbonyl-Selenido Complex of Manganese," *Angewandte Chemie International Edition* 35 (1996): 1710–1712.

21. P. A. Sobov, A. F. Shestakov, A. V. Kuzmin, et al., "A Dimer of the Negatively Charged Carbonyl Cluster $\{Ir_4(CO)_{11}^-\}_2$ Bonded by a Single Ir–Ir Bond, and Comparison with the Singly Bonded $(C_{60}^-)_2$ Dimer," *Zeitschrift Fur Anorganische Und Allgemeine Chemie* 649 (2023): e202200368.

22. L. F. Dahl and R. E. Rundle, "The Crystal Structure of Dimanganese Decacarbonyl $Mn_2(CO)_{10}$," *Acta Crystallographica* 16 (1963): 419–426.

23. F. Pioneau, A. P. Sattelberger, E. Lu, and S. T. Liddle, *Molecular Metal-Metal Bonds Compounds: Synthesis, Properties* (Wiley-VCH, 2015).

24. L. P. H. Lopez, R. R. Schrock, and P. Müller, "Dimers that Contain Unbridged W(IV)/W(IV) Double Bonds," *Organometallics* 25 (2006): 1978–1986.

25. J. C. Green, M. L. H. Green, and G. Parkin, "The Occurrence and Representation of Three-Centre Two-Electron Bonds in Covalent Inorganic Compounds," *Chemical Communications* 48 (2012): 11481–11503.

26. C. Lepetit, P. Fau, K. Fajerwerg, M. L. Kahn, and B. Silvi, "Topological Analysis of the Metal-Metal Bond: A Tutorial Review," *Coordination Chemistry Reviews* 345 (2017): 150–181.

27. S. M. Tiefenthaler, F. Kleemiss, and N. Korber, "$[A([18]crown-6)]_2[Pt(CO)_3]\cdot 10\ NH_3$ (A=K, Rb) – A Crystal Structure Containing the Long Postulated $[Pt(CO)_3]$," *Zeitschrift Fur Anorganische Und Allgemeine Chemie* 2 (2022): 648.

28. L. Hackspill, "Sur Quelques Propriétés Des métaux Alcalins," *Helvetica Chimica Acta* 11 (1928): 1003–1026.

29. R. B. King and A. Fronzaglia, "Organometallic Chemistry of the Transition Metals. XV. New Olefinic and Acetylenic Derivatives of Tungsten," *Inorganic Chemistry* 5 (1966): 1837–1846.

30. CrysAlisPro171.43.143a, Oxford Diffraction, Agilent Technologies 2021.

31. G. M. Sheldrick, "SHELXT - Integrated Space-Group and Crystal-Structure Determination," *Acta Crystallographica Section A* 71 (2015): 3–8.

32. G. M. Sheldrick, "Crystal Structure Refinement with SHELXL," *Crystal Structure Communications* 71 (2015): 3–8.

33. O. V. Dolomanov, L. J. Bourhis, R. J. Gildea, J. A. K. Howard, and H. Puschmann, "OLEX2: A Complete Structure Solution, Refinement and Analysis Program," *Journal of Applied Crystallography* 42 (2009): 339–341.

34. Diamond 5, Crystal Impact, H. Putz, K. Brandenburg 2024.

35. F. Neese, "The ORCA Program System," *Wiley Interdisciplinary Reviews Computational Molecular Science* 2 (2012): 73–78.

36. F. Neese, "Software Update: The ORCA Program System—Version 5.0," *Wiley Interdisciplinary Reviews Computational Molecular Science* 12 (2022): e1606.

37. A. D. Becke, "Density-Functional Thermochemistry. III. The Role of Exact Exchange," *Chemical Physics* 98 (1993): 5648–5652.

38. C. Lee, W. Yang, and R. G. Parr, "Development of the Colle-Salvetti Correlation-Energy Formula into a Functional of the Electron Density," *Physical Review B* 37 (1988): 785–789.

39. S. H. Vosko, L. Wilk, and M. Nusair, "Accurate Spin-Dependent Electron Liquid Correlation Energies for Local Spin Density Calculations: A Critical Analysis," *Canadian Journal of Physics* 58 (1980): 1200–1211.

40. P. J. Stephens, F. J. Devlin, C. F. Chabalowski, and M. J. Frisch, "Ab Initio Calculation of Vibrational Absorption and Circular Dichroism Spectra Using Density Functional Force Fields," *The Journal of Physical Chemistry* 98 (1994): 11623–11627.

41. D. A. Pantazis, X.-Y. Chen, C. R. Landis, and F. Neese, "All-Electron Scalar Relativistic Basis Sets for Third-Row Transition Metal Atoms," *Journal of Chemical Theory and Computation* 4 (2008): 908–919.

42. F. Weigend and R. Ahlrichs, "Balanced Basis Sets of Split Valence, Triple Zeta Valence and Quadruple Zeta Valence Quality for H to Rn: Design and Assessment of Accuracy," *Physical Chemistry Chemical Physics* 7 (2005): 3297–3305.

43. M. Garcia-Ratés and F. Neese, "Effect of the Solute Cavity on the Solvation Energy and Its Derivatives Within the Framework of the Gaussian Charge Scheme," *Journal of Computational Chemistry* 41 (2020): 922–939.

44. T. Lu, "A Comprehensive Electron Wavefunction Analysis Toolbox for Chemists, Multiwfn," *The Journal of Chemical Physics* 161 (2024): 082503.

45. W. Humphrey, A. Dalke, and K. Schulten, "VMD: Visual Molecular Dynamics," *Journal of Molecular Graphics* 14 (1996): 33–38.

Supporting Information

The supporting information contains crystallographic data tables, interatomic distances from the crystal structures, calculated interatomic distances and unit cell pictures of (1) and (2), as well as the cationic environment of (2). Additional supporting information can be found online in the Supporting Information section. **Supporting Fig. S1:** Unit cell of $[Rb[2.2.2]crypt]_2[Mn_2(CO)_8] \cdot 4NH_3$ along the crystallographic a-axis (left) and the crystallographic c-axis (right). For clarity, the hydrogen atoms of [2.2.2]crypt are omitted and it is shown as wires and sticks. Displacement ellipsoids are shown at 50% probability. **Supporting Fig. S2:** Cationic environment in $[K[18]crown\text{-}6]_2K_2[W_2(CO)_8] \cdot 14NH_3$. Displacement ellipsoids are shown at 50% probability. **Supporting Fig. S3:** Unit cell of $[K[18]crown\text{-}6]_2K_2[W_2(CO)_8] \cdot 14NH_3$ along the crystallographic a-axis (left) and the crystallographic *b*-axis (right). For clarity, the hydrogen atoms of [18]crown-6 are omitted and it is shown as wires and sticks. Displacement ellipsoids are shown at 50% probability. **Supporting Fig. S4:** Optimized geometries of $[Mn_2(CO)_8]^{2-}$ (left) and $[W_2(CO)_8]^{4-}$ (right). **Supporting Table S1:** Crystallographic data of $[Rb[2.2.2]crypt]_2[Mn_2(CO)_8] \cdot 4NH_3$. **Supporting Table S2:** Selected interatomic distances in $[Rb[2.2.2]crypt]_2[Mn_2(CO)_8] \cdot 4NH_3$. **Supporting Table S3:** Crystallographic data of $[K[18]crown\text{-}6]_2K_2[W_2(CO)_8] \cdot 14NH_3$. **Supporting Table S4:** Selected interatomic distances in $[Rb[2.2.2]crypt]_2[Mn_2(CO)_8] \cdot 4NH_3$. **Supporting Table S5:** Calculated interatomic distances in $[Mn_2(CO)_8]^{2-}$. **Supporting Table S6:** Calculated interatomic distances in $[W_2(CO)_8]^{4-}$.